How to Detect Water in the Mantle Wedge of a Subduction Zone Using Seismic Anisotropy

E. Kaminski, D. A. Okaya

HAL Id: insu-03589304
https://insu.hal.science/insu-03589304

Submitted on 25 Feb 2022

Geophysical Research Letters

Key Points:
- Development of trench-parallel anisotropy in a mantle wedge is modeled using a model of crystals deformation and dynamic recrystallization
- Progressive hydration toward the trench produces a "morph zone" with a weak anisotropy and a decrease of VP and VS
- Applied to the Lau Basin the model shows that water rather than trench-parallel flow explain the evolution of seismic anisotropy there

Correspondence to:
E. Kaminski,
kaminski@ipgp.fr

How to Detect Water in the Mantle Wedge of a Subduction Zone Using Seismic Anisotropy

E. Kaminski[1] and **D. A. Okaya[2]**

[1]Institut de physique du globe de Paris, Sorbonne Paris Cité, CNRS, University Paris Diderot, Paris, France, [2]Department of Earth Sciences, University of Southern California, Los Angeles, CA, USA

Abstract In approximately one fourth of worldwide subduction zones, seismic observations indicate a rotation from trench-normal to trench-parallel fast axis orientations in the mantle wedge. To interpret this observation we predict the evolution of crystal lattice preferred orientation in mantle wedge material as a function of the amount of water by using a model of polycrystal deformation (D-Rex) coupled with an analytical corner flow. The resulting seismic signature is obtained from synthetic seismic wave propagation through this mantle wedge. We identify that progressive hydration produces the rotation of fast axis orientations and can generate between the two zones of trench-parallel and trench-normal fast axis orientations a morph zone with very small anisotropy and a related decrease in *P* and *S* wave velocities. Such a morph zone is not produced by trench-parallel flow, hence this signature can be used to detect water in the mantle wedge.

Plain Language Summary A subduction zone's mantle wedge can have a complex pattern of seismic anisotropy where the fast direction often rotates from trench-parallel close to the trench to trench-normal in the backarc. This pattern can be interpreted as induced by either 3-D trench-parallel flow or by the presence of water close to the trench. Almost all models so far favored the trench-parallel flow hypothesis, usually based on indirect or complementary indicators such as the evolution of geochemical signatures of volcanoes along the arc. Here we examine a seismic anisotropy observational signature that can be used to discriminate between the two explanations. The concept is defined using an interdisciplinary approach linking a direct modeling of the flow in the subduction wedge and a computation of seismic wave propagation in anisotropic media. We define a unique water-induced signature that is the presence of a "morph zone" characterized by a weak anisotropy and a decrease of seismic velocities. We apply the model to the Lau Basin where we find this predicted signature, demonstrating for the first time that water rather than trench-parallel flow is responsible for the observed anisotropy pattern there.

1. Introduction

Seismic anisotropy is a unique tool that can be used to infer the existence of upper mantle flow (Long & Becker, 2010; Montagner, 2007) and to detect water in the convective upper mantle (e.g., Karato, 2003). Most studies of the link between seismic anisotropy and mantle flow have focused on subduction zones (e.g., Long & Silver, 2008; Long & Wirth, 2013). Whereas flow in the mantle wedge was initially modeled as a 2-D corner flow that is driven by the subducting plate (Figure 1a), the discovery of trench-parallel seismic anisotropy was interpreted as the result of trench-parallel flow below the slab (Russo & Silver, 1994) or in the mantle wedge (Abt et al., 2009; Mehl et al., 2003; Figure 1b). But experimental laboratory studies of the development of lattice preferred orientation (LPO) in olivine aggregates have shown that it is also possible to produce seismic anisotropy with an orientation normal to the shear direction in the presence of water (Jung & Karato, 2001; Lassak et al., 2006; Figure 1c).

The effect of water on olivine LPO is not unique and depends on (a) temperature, (b) the amount of water, and (c) the condition of stress level. Among the five types of olivine LPO that have been identified so far (types A, B, C, D, and E, Katayama et al., 2004), the three relevant for the mantle wedge are type A for dry conditions, type B for wet conditions and large stress, and type C for wet conditions and low stress (e.g., Jung & Karato, 2001; Katayama & Karato, 2006). In subduction zones where the wedge flow field is physically trench-normal, trench-normal LPO will correspond to type A or type C, that is, seismic *P* and *S* wave fast direction normal to the trench. In contrast, trench-parallel LPO will correspond to type B, that
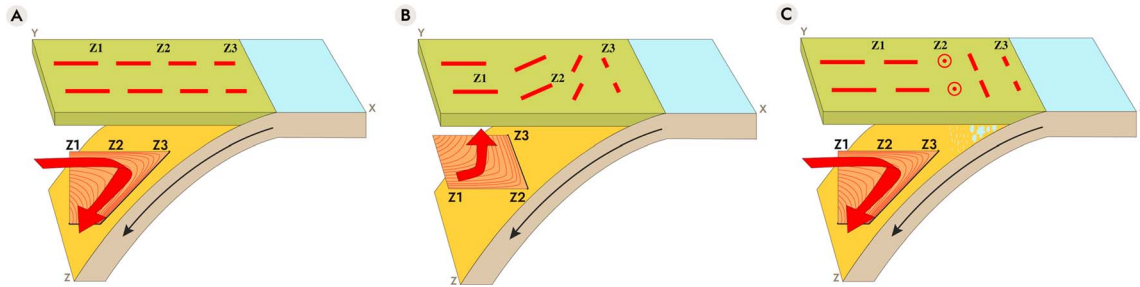
Figure 1. End-members models of mantle flow in the mantle wedge of a subduction zone and their associated seismic anisotropy. Red bars on surface are seismic shear wave splitting fast bars that denote fast direction and δt magnitude; circles are null values. (a) Trench perpendicular flow involving only dry crystals and producing trench-normal seismic anisotropy. (b) Trench-parallel flow close to the trench producing trench-parallel seismic anisotropy. (c) Trench perpendicular flow involving both dry and wet crystals. Three zones (Z1, Z2, and Z3) are introduced to describe the evolution of anisotropy as a function of the distance from the trench. In case (a) δt decreases but the fast direction is constant over the three zones. In both cases (b) and (c) the shear wave splitting signature becomes trench-parallel in zone 3. The key difference between case (b) and (c) is observed in zone 2.

is, seismic wave fast direction parallel to the trench (Kneller et al., 2005; Kneller & van Keken, 2008; Lassak et al., 2006). The seismic attributes of Type C LPO are different from those of Types A and B (Figure 2) and could bear important consequences for the detection of water.

In this study, we examine LPO evolution as incoming mantle wedge flow is subjected to increasing stress and hydration. We describe the role of type C LPO as a transition from type A to type B LPO and we calculate synthetic shear wave splitting in order to predict the associated observable patterns. We obtain a unique seismic signature of progressive hydration that can be used to infer the presence of water in the mantle wedge. The model is successfully applied to the Lau back-arc basin.
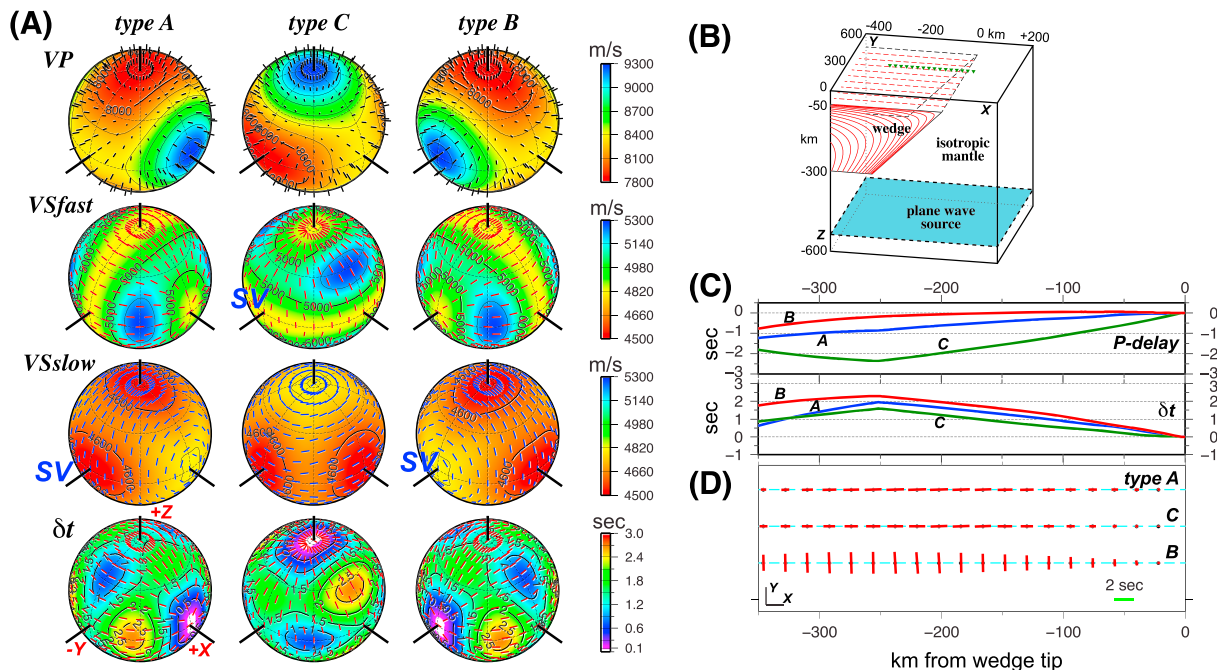

Figure 2. Signature of three main types of fluid-affected olivine LPO within a mantle wedge (types A, C, B). (a) Seismic velocities for P wave (VP), fast S wave (VSfast), slow S wave (VSslow), and shear wave delay time (δt). Spherical coordinates represent seismic wave propagation direction. Wave polarization directions shown as bars (P = black, Sfast = red, Sslow = blue, δt fast shear = red). "SV" label denotes which of fast or slow VS has predominant vertical shear motion for horizontal propagation. (b) Seismic model used to compute synthetic seismograms. Green triangles represent "array" collecting upcoming teleseismic shear wave. (c) Predicted observables for LPO produced by corner flow of each main type of olivine: (top) P-delay with respect to isotropic mantle velocity; (bottom) shear wave delay time. (d) Synthetic seismogram shear wave splitting response of mantle wedges composed purely of one type of LPO. Splitting bars shown in map view across linear array. Each synthetic split bar is an average of 36 back azimuths. LPO = lattice preferred orientation.

2. Methods

To model the seismic signature of the flow in a mantle wedge as a function of water content and stress, we first define a 2-D mantle wedge flow field for a 45° dipping slab, using the similarity solution of the steady incompressible Stokes equation for a slow corner flow of a Newtonian fluid (Batchelor, 1967; Ribe, 1989). This provides both the velocity field and the velocity gradient tensors required to compute the LPO. This calculation is dimensionless and does not require specification of plate velocities.

We calculate LPO evolution at all points uniformly distributed throughout the 2-D mantle wedge. The evolution of crystal aggregate elastic tensors in the wedge is calculated along pathlines taken by the aggregates that are composed of 70 wt.% olivine and 30 wt.% enstatite, a typical first order approximation for a harzburgite (Ribe, 1992). The aggregates' deformation and associated LPO evolution by plastic deformation and dynamic recrystallization are modeled using the software code D-Rex (Kaminski et al., 2004) as detailed in the supporting information. The result of these calculations is a uniformly gridded mantle wedge composed of strained LPO elastic tensors inserted into a 2-D Earth model cross section projected into a 3-D volume (Figure 2 and supporting information).

We calculate the magnitudes of predicted seismic observables of P wave arrival delay time and S wave delay time using the Earth cross-section (Figure 2c and online supporting information). We also generate waveform synthetic seismograms of an upcoming teleseismic wave through the wedge by using a 3-D anisotropic finite difference wave propagation code (Levin et al., 2007; Okaya & McEvilly, 2003) as detailed in the supporting information. The synthetic seismograms are then analyzed for shear wave splitting using the Menke-Levin cross-correlation splitting method (Menke & Levin, 2003) to derive delay time δt and fast-S direction ϕ (see supporting information).

3. Results

3.1. Incoming Wedge Flow of Pure LPO Types

For calibration purposes, we first compute the seismic anisotropy signature of each pure type of LPO produced during trench-normal flow: (a) dry (all type A), (b) wet and high stress (all type B), and (c) wet and low stress (all type C). The calculation of the LPO evolution along the pathlines starts at a distance $x = -750$ km from the trench, with uniformly random orientations of the crystals in the aggregates. After about 100 km the LPO reaches a plateau, which insures that the initial condition does not affect the calculation of LPO evolution in the wedge.

Figure 2a illustrates for the three LPO types (A-B-C) their Christoffel seismic P wave and two S wave velocities, shear wave delay times δt, and associated fast and slow particle motions on the surface of spheres whose coordinates represent all propagation directions (azimuth and inclination angles). The LPO are presented with their X-axes aligned in the mantle wedge flow direction. As expected, for near-vertical propagation of teleseismic waves (Z-axes of spheres), the direction of shear wave fast propagation, ϕ, is aligned with the shear direction for type A, and normal to the shear direction for type B. The case of type C is distinctive in that in the near-vertical propagation direction, VP is fast, δt approaches zero (null), and ϕ mimics the incoming wave's back azimuth. Upon shearing due to flow, this type's LPO will develop moderate trench-parallel δt-ϕ splitting values in the vertical direction.

Figure 2c shows the predicted seismic signal for each sing type of LPO (A, B, and C) and Figure 2d shows the δt-ϕ splitting parameters derived from the synthetic seismograms. The uniform conditions yield consistent patterns of anisotropy: split bars are normal (A, C) or parallel (B) to the trench in accordance to the type of LPO, and the delay times decrease toward the trench as the mantle wedge thins. The variation of the delay time further reflects the contribution of the two major anisotropic regions that develop under the upper plate and above the downgoing subduction slab (Figure S1). As expected from the seismic velocities shown in Figure 2a, the delay times are a bit smaller for type C compared to type A (see Figure S1). In the three LPO cases the downgoing mantle wedge flow contributes significantly to the shear wave splitting amounts and explains the variation of the delay time that otherwise would be constant. For type C in Figure 2d, nearly all of the splitting originates from the downgoing flow; the incoming flow toward the trench contributes little splitting in accordance with Figure 2a (i.e., see Figure S1c).
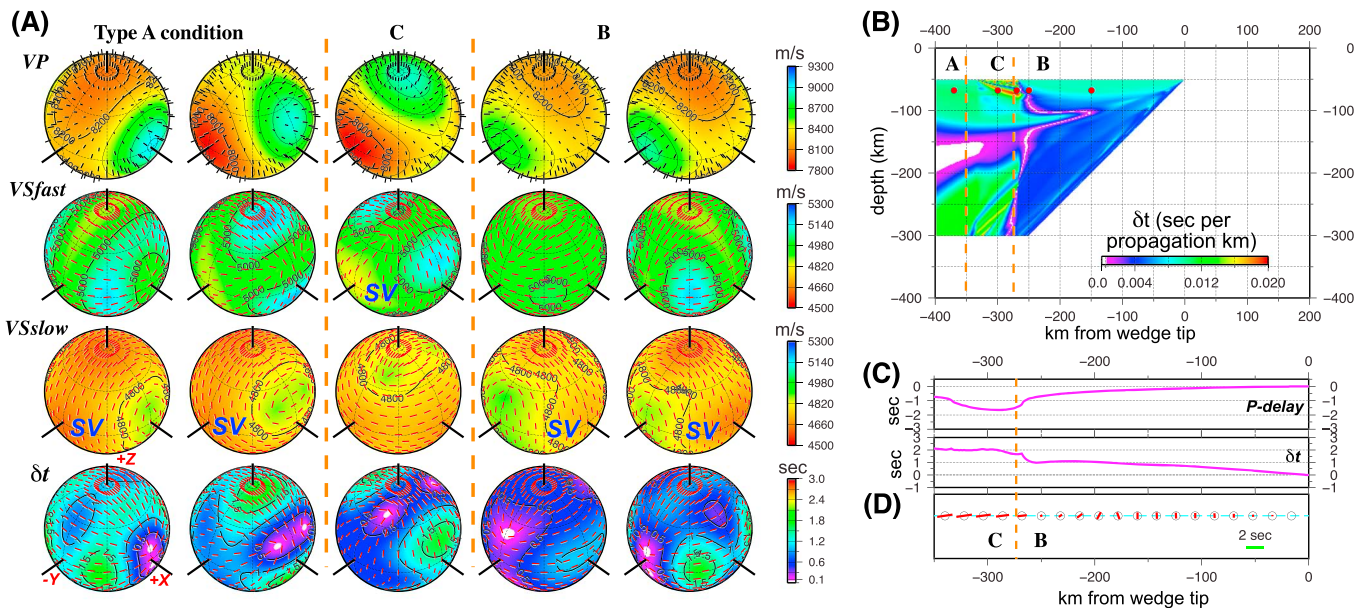
Figure 3. Evolution of LPO with progressive hydration and increased stress, from type A to C to B and associated seismological observable characteristics. (a) Velocity/delay time spheres for five points in LPO field. Particle motion bars and SV label as defined in Figure 2. (b) Cross-section of mantle wedge showing shear wave splitting, δt, per propagation kilometers in vertical direction. Red dots indicate locations of points in (a). (c) Predicted observables of P-delay and δt for this LPO field. (d) Shear wave splitting response for upward propagating synthetic teleseismic wave. The dashed orange lines mark the transitions between dry (a), wet/low stress (c), and wet/high stress (b) LPO conditions. The horizontal scales, hence the position of the orange lines, are different in (b) and in (c)–(d). A null region is produced at the type C-to-B transition corresponding to the "morph" zone. LPO = lattice preferred orientation.

3.2. Transitions of LPO Due to Progressive Hydration and Stress Increase Toward the Trench

To reproduce the water-induced evolution of LPO expected in subduction zones, we consider a simple scenario of progressive hydration and stress increase in the mantle wedge toward the trench. In the upper part of the mantle flow, the LPO will laterally evolve from type A (dry) to type C (wet/low stress) and eventually to type B (wet/high stress), whereas the evolution will be reversed in the downgoing wedge flow.

Figure 3 shows the lateral transition of LPO types and related modification of seismic velocities and shear wave splitting parameters. The region corresponding to type C LPO is characterized by a weak anisotropy. This is due to two reasons: (i) The difference of shear wave propagation velocity in the vertical direction is the smallest for type C LPO. (ii) The lateral type C region is located between the dry (>350 km) and wet regions (<275 km) that correspond to LPO zones A and B, respectively, hence is a transition or "morph" zone between the zones where the seismic observations would correspond to trench-normal and trench-parallel fast axis orientations, respectively. Deformation in the morph zone must first erase the type A LPO before producing type C LPO, which itself is erased when entering the wet region corresponding to type B LPO. This is why the morph zone is not perfectly vertically aligned with the zone in the wedge where the deformation parameters of olivine polycrystals correspond to type C (km = 350–275). This double evolution in a relatively short distance prevents the development of a dominant type C LPO. Hence, the morph zone due to progressive hydration and stress increase in the mantle wedge produces a low anisotropy channel characteristic of the presence of water; this is demonstrated in the synthetic splitting bars in Figure 3d. In contrast, the rotation of anisotropy due to dry trench-parallel flow is laterally sharp and does not generate such a low anisotropy channel (Menke et al., 2015).

The velocity spheres in Figures 2 and 3 further suggest that the evolution of the splitting parameters will correlate with a transition from slower SV in the horizontal directions (type A LPO corresponding to dry back-arc LPO) to faster SV (type C LPO in the morph zone) and back to slower SV (type B LPO) close to the trench (see "SV" in Figures 2a and 3a). While these shear vertical motions are obtained from Christoffel equations for shear body waves, we note that SV and SH surface waves must respond to the same LPO structure, although with less vertical and lateral resolution. This provides a complimentary signature of the effect of water on seismic anisotropy. In contrast, the evolution from trench-normal to
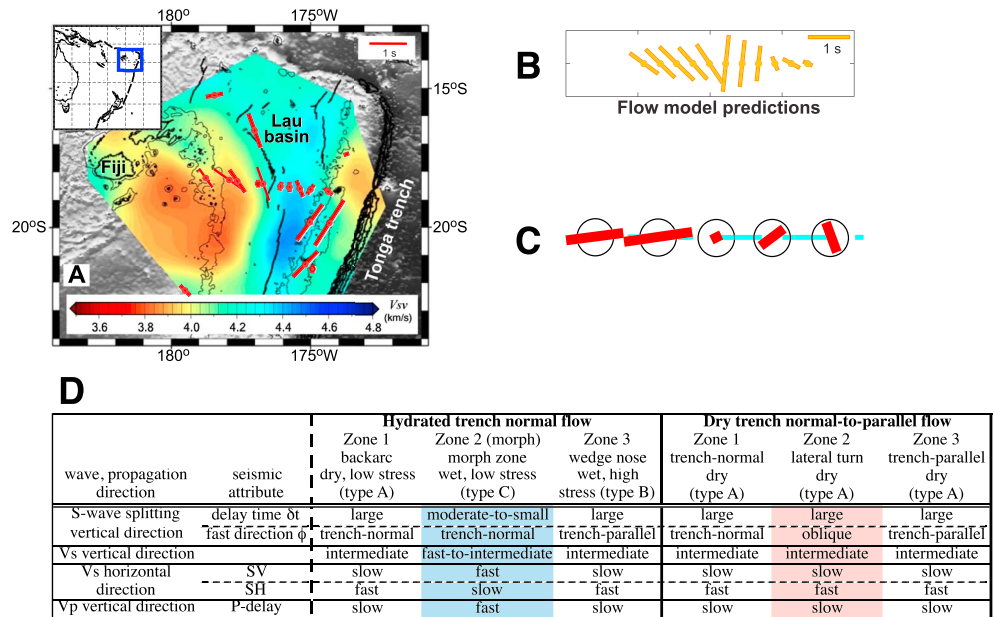
Figure 4. Seismic observables in the Lau back-arc basin. (a) Shear wave delay times (red bars) from Smith et al. (2001) and azimuthally averaged surface wave SV velocities at 100 km depth from Wei et al. (2015). Inset: location of Lau basin in southwest Pacific. The two patterns of observables are fully consistent with the presence of the "morph" zone predicted by our model of water-induced anisotropy. (b) The shear wave splitting predictions by Conder and Wiens (2007) reproduce the rotation of lattice preferred orientation from trench-parallel to trench-normal, but are not consistent with the drop in intensity of anisotropy in the morph zone. The trench-parallel flow hypothesis also does not address the lateral spatial patterns of Vsv in the mantle wedge. (c) This study's synthetic predictions of the model with the presence of a low anisotropy morph zone. (d) Seismological observable characteristics of a hydrated trench-normal flow (Figure 1c) versus a dry flow that becomes trench-parallel close to the trench (Figure 1b). Each flow scenario has three spatial zones that represent incoming portions of the mantle wedge flow (Z1–Z3 in Figure 1). Large/small and slow/fast are relative magnitudes within one lateral set of zones. The signature of the hydrated trench-parallel flow is consistent with the Lau basin observations.

trench-parallel of only dry flow will yield relative uniform averaged slow SV at all distances from the trench.

3.3. Application to Lau Basin

We summarize in Figure 4d the seismological observable characteristics that can be used to discriminate an interpretation of trench-parallel flow with hydration of the mantle wedge from dry trench-parallel flow. The Lau back-arc basin is a representative example of the pattern of azimuthal anisotropy in a subduction zone where we can perform his examination. Here we will compare our model predictions to the data of Smith et al. (2001) that were obtained from splitting analysis of local earthquakes that sample the wedge. The pattern of LPO evolution is thus expected to be similar to the one predicted by progressive hydration in Figure 3 where we have used SKS waves while putting aside any contributions from the slab and subslab mantle.

Lau basin offers a detailed image of the rotation of seismic anisotropy with distance from the trench (Figure 4). The shear wave splitting fast directions are oblique-to-normal to the Tonga trench at distances >400 km from the trench, and is observed to be trench-parallel ~100 km from the trench (Smith et al., 2001). Also shown in Figure 4 are azimuthally averaged vertical-polarization shear wave (SV) velocities that were derived from earthquake surface waves and ambient noise tomography (Wei et al., 2015). These SV velocities in the upper mantle wedge (100 km depth) are slower at distances >400 km from the trench and close to the trench, with a faster SV zone in-between. We note that the data and methods of Wei et al. (2015) emphasized seismic velocities for horizontally traveling seismic waves whereas the shear wave splitting was based on anisotropic seismic velocities in the near-vertical direction (upward teleseismic waves).

In this area seismic observations of trench-parallel fast axis orientations have been interpreted as trench-parallel flow due to an infiltration of the Samoan plume that could produce a southward flow in the

asthenosphere (Smith et al., 2001). However, this model requires a fast flow ($\approx$50 cm/year; Conder & Wiens, 2007) focused in a somewhat ad hoc low viscosity channel. Such extreme characteristics seem at odds with the relatively small buoyancy flux associated with the hotspot and the specific pattern of anisotropy expected for a plume spreading below the lithosphere (e.g., Kaminski & Ribe, 2002) not observed in the Lau basin. Last, the trench-parallel flow model fails to account for the decrease of anisotropy in the zone where the anisotropy transitions from trench-parallel to trench-normal that is observed in the Lau Basin (Figure 4b, Conder & Wiens, 2007). Inclusion of a back-arc spreading center and an imposed trench-parallel flow in the modeling also does not produce the transition zone of weak anisotropy either (Menke et al., 2015).

Comparison between our model predictions for progressive hydration (Figure 4d) and observation in Lau basin (Figure 4a) shows that the two patterns are similar. The presence of the morph zone predicted in our concept is marked both by the weak anisotropy associated with the rotation from trench-parallel to trench-normal, as well as the evolution of horizontal-direction averaged SV from slow to fast to slow again. Finally, we note that the lateral extent of the morph zone, that in our model marks the beginning of the hydration of the olivine crystals, corresponds well to the "seismic belt" recently detected in the area and interpreted as the signature of metamorphic dehydration in the slab (see Figure 1 of Wei et al., 2017). Progressive hydration thus provide a better explanation for the complex seismic anisotropy pattern observed in the Lau basin compared to trench-parallel flow. The detection of water by our method supports the conclusion reached by the recent studies of Wei et al. (2015, 2017) based on independent manifestations of the presence of water.

4. Discussion

We have shown that progressive hydration/stress increase toward the trench should produce, within the framework of trench perpendicular corner flow, a morph zone at the transition in-between the two zones where seismic observations correspond to trench-normal and trench-parallel fast axis orientations. The origin of the morph zone is twofold: (a) it corresponds to the "destruction" of coherent type A LPO and "reconstruction" of coherent type B LPO, and (c) it corresponds to the expression of the characteristics of type C LPO which yields a null delay time in vertical seismic propagation direction. The presence of the morph zone is a key difference between water-induced and flow-induced rotation of seismic anisotropy. In this latter case of trench-parallel flow, a simple rotation of seismic anisotropy without a decrease of delay time is expected.

A robust diagnosis of the presence of water will depend on the width of the morph zone. The larger the zone with water content or stress level corresponding to type C LPO, the wider the morph zone and the easier its seismic detection. If the region is too narrow to allow for a coherent expression of pure type C characteristics, a morph zone of minimal lateral extent will be always present due to the transition between type A and type B fabrics. The width of the transition between the fabric types depends on the ease of dynamic recrystallization to erase the type A fabric and to produce the new fabric under the conditions of the new (increased) water content and stress. This mechanical efficiency is primarily controlled by the rate of grain boundary migration, as quantified by the value of the parameter M* in D-Rex (supporting information). We have used here a value of 125 for M* based on uniform deformation experiments (Kaminski & Ribe, 2001). Recent studies however suggest that M* = 10 is more appropriated for fabric evolution in nonuniform deformation (Boneh et al., 2015; Hedjazian et al., 2017). For such a small value of M* the morph zone will be wider than 50 km and hence always seismically detectible.

The detection of the morph zone primarily relies on the decrease of delay time spatially next to the rotation of seismic anisotropy direction. However, as summarized in Figure 4d, other seismic observables can be used to confirm the presence of the morph zone. *P* wave oblique paths and horizontal surface waves will be sensitive to A-C-B structure. For detection of water in the mantle wedge, we recommend that future campaigns of seismic data acquisition should include both surface and body waves. Reviewing some recent studies, we suggest three places in which the presence of a morph zone—hence of water—is consistent with the seismic observations. In the southern part of the Apenninic-Tyrrhenian domain (Italy), a narrow channel of weak anisotropy is found between two zones of seismic observations of trench-normal fast axis orientations north of the Aeolian Islands and trench-parallel fast axis orientations along the Calabria coast (Baccheschi et al., 2011; Margheriti et al., 2003). In the northern Honshu arc, a channel of low seismic anisotropy locally marks the transition between areas of trench-normal and trench-parallel seismic fast directions (Huang et al., 2011). In the Ryukyu subduction, a transition between seismic observations of trench-normal and trench-

parallel fast axis orientations corresponds to a zone of small anisotropy where the determination of the direction of fast propagation is not possible (Kuo et al., 2012). Collection of additional data as suggested by our method could confirm the presence of the morph zone in these areas.

In contrast, in some areas in Central America where trench-parallel flow is the favored hypothesis to explain trench-parallel anisotropy, the transition between trench-normal and trench-parallel anisotropy is laterally sharp and does not undergo a low anisotropy transition (Abt et al., 2009). The presence of water is not excluded in the case of trench-parallel flow. But its seismic signature will be less straightforward, and the interpretation of this combined case will require both 3-D numerical modeling of the flow (e.g., Faccenda & Capitanio, 2013) and detailed 3-D mapping of anisotropic structures in the mantle wedge (e.g., Abt et al., 2009).

5. Conclusion

We have characterized in this article the seismic signature of progressive hydration in the mantle wedge toward the trench and how this hydration can be detected using shear wave splitting parameters. The key observation is weak seismic anisotropy that marks a transitional morph zone. Horizontal propagation-based SV tomography has its own spatial hydration pattern, and if present together with the morph zone may confirm the presence of water. Such a morph zone and the results of SV tomography allowed us to infer the presence of water in the Lau basin mantle wedge (Figure 4). Future campaigns of data acquisition in subduction zones should measure both shear wave splitting δt-ϕ, shear wave tomography values, and teleseismic P-delay, in order to firmly assess the presence of water based on seismic measurements.

References

Abt, D. L., Fischer, K. M., Abers, G. A., Strauch, W., Protti, J. M., & Gonzalez, V. (2009). Shear-wave anisotropy beneath Nicaragua and Costa Rica: Implications for flow in the mantle wedge. *Geochemistry, Geophysics, Geosystems*, *10*, Q05S15. https://doi.org/10.1029/2009GC002375

Baccheschi, P., Margheriti, L., Steckler, M. S., & Boschi, E. (2011). Anisotropy patterns in the subducting lithosphere and in the mantle wedge: A case study—The southern Italy subduction system. *Journal of Geophysical Research*, *116*, B08306. https://doi.org/10.1029/2010JB007961

Batchelor, G. K. (1967). *An introduction to fluid dynamics*. New York: Cambridge Univ. Press.

Boneh, Y., Morales, L., Kaminski, E., & Skemer, P. (2015). Modeling olivine CPO evolution with complex deformation histories: Implications for the interpretation of seismic anisotropy in the mantle. *Geochemistry, Geophysics, Geosystems*, *16*, 3436–3455. https://doi.org/10.1002/2015GC005964

Conder, J. A., & Wiens, D. A. (2007). Rapid mantle flow beneath the Tonga volcanic arc. *Earth and Planetary Science Letters*, *264*, 299–307. https://doi.org/10.1016/j.epsl.2007.10.014

Faccenda, M., & Capitanio, F. A. (2013). Seismic anisotropy around subduction zones: Insights from three-dimensional modeling of upper mantle deformation and SKS splitting calculations. *Geochemistry, Geophysics, Geosystems*, *14*, 243–262. https://doi.org/10.1029/2012GC004451

Hedjazian, N., Garel, F., Davies, D. R., & Kaminski, E. (2017). Age-independent seismic anisotropy under oceanic plates explained by strain history in the asthenosphere. *Earth and Planetary Science Letters*, *460*, 135–142. https://doi.org/10.1016/j.epsl.2016.12.004

Huang, Z., Zhao, D., & Wang, L. (2011). Seismic heterogeneity and anisotropy of the Honshu arc from the Japan Trench to the Japan Sea. *Geophysical Journal International*, *184*, 1428–1444. https://doi.org/10.1111/j.1365-246X.2011.04934.x

Jung, H., & Karato, S. I. (2001). Water-induced fabric transitions in olivine. *Science*, *293*, 1460–1463. https://doi.org/10.1126/science.1062235

Kaminski, E., & Ribe, N. (2001). A kinematic model for recrystallization and texture development in olivine polycrystals. *Earth and Planetary Science Letters*, *189*, 253–267. https://doi.org/10.1016/S0012-821X(01)00356-9

Kaminski, E., & Ribe, N. (2002), Time scales for the evolution of seismic anisotropy in mantle flow. *Geochemistry, Geophysics, Geosystems*, *3*(8), https://doi.org/10.1029/2001GC000222, 1051

Kaminski, E., Ribe, N., & Browaeys, J. T. (2004). D-Rex, a program for calculation of seismic anisotropy due to crystal lattice preferred orientation in the convective upper mantle. *Geophysical Journal International*, *158*, 744–752. https://doi.org/10.1111/j.1365-246X.2004.02308.x

Karato, S. (2003). Mapping water content in Earth's upper mantle. In J. E. Eiler (Ed.), *Inside the subduction factory* (pp. 135–152). Washington DC: American Geophysical Union. https://doi.org/10.1029/138GM08

Katayama, I., Jung, H., & Karato, S.-I. (2004). New type of olivine fabric from deformation experiments at modest water content and low stress. *Geology*, *32*, 1045–1048. https://doi.org/10.1130/G20805.1

Katayama, I., & Karato, S.-I. (2006). Effect of temperature on the B- to C-type olivine fabric transition and implication for flow pattern in subduction zones. *Physics of the Earth and Planetary Interiors*, *157*, 33–45. https://doi.org/10.1016/j.pepi.2006.03.005

Kneller, E. A., & van Keken, P. E. (2008). The effects of three-dimensional slab geometry on deformation in the mantle wedge: Implications for shear wave anisotropy. *Geochemistry, Geophysics, Geosystems*, *9*, Q01003. https://doi.org/10.1029/2007GC001677

Kneller, E. A., van Keken, P. E., Karato, S., & Park, J. (2005). B-type olivine fabric in the mantle wedge: Insights from high-resolution non-Newtonian subduction zone models. *Earth and Planetary Science Letters*, *237*, 781–797. https://doi.org/10.1016/j.epsl.2005.06.049

Kuo, B. Y., Wang, C. C., Lin, S. C., Lin, C. R., Chen, P. C., Jang, J. P., & Chang, H. K. (2012). Shear-wave splitting at the edge of the Ryukyu subduction zone. *Earth and Planetary Science Letters*, *355-356*, 262–270. https://doi.org/10.1016/j.epsl.2012.08.005

Lassak, T. M., Fouch, M. J., Hall, C. E., & Kaminski, E. (2006). Seismic characterization of mantle flow in subduction systems: Can we resolve a hydrated mantle wedge? *Earth and Planetary Science Letters*, *243*, 632–649. https://doi.org/10.1016/j.epsl.2006.01.022

Levin, V., Okaya, D., & Park, J. (2007). Cause and effect: Shear wave birefringence in wedge-shaped anisotropic regions. *Geophysical Journal International*, *168*, 275–286. https://doi.org/10.1111/j.1365246X.2006.03224.x

Long, M. D., & Becker, T. W. (2010). Mantle dynamics and seismic anisotropy. *Earth and Planetary Science Letters*, *297*, 341–354. https://doi.org/10.1016/j.epsl.2010.06.036

Long, M. D., & Silver, P. G. (2008). The subduction zone flow field from seismic anisotropy: A global view. *Science*, *319*, 315–318. https://doi.org/10.1126/science.1150809

Long, M. D., & Wirth, E. A. (2013). Mantle flow in subduction systems: The mantle wedge flow field and implications for wedge processes. *Journal of Geophysical Research: Atmospheres*, *118*, 583–606. https://doi.org/10.1002/jgrb.50063

Margheriti, L., Lucente, F. P., & Pondrelli, S. (2003). SKS splitting measurements in the Apenninic-Tyrrhenian domain (Italy) and their relation with lithospheric subduction and mantle convection. *Journal of Geophysical Research*, *108*(B4), 2218. https://doi.org/10.1029/2002JB001793

Mehl, L., Hacker, B. R., Hirth, G., & Kelemen, P. B. (2003). Arc-parallel flow within the mantle wedge: Evidence from the accreted Talkeetna arc, south central Alaska. *Journal of Geophysical Research*, *108*(B8), 2375. https://doi.org/10.1029/2002JB002233

Menke, W., & Levin, V. (2003). The cross-convolution method for interpreting SKS splitting observations, with application to one and two layer anisotropic earth models. *Geophysical Journal International*, *154*, 379–392. https://doi.org/10.1046/j.1365-246X.2003.01937.x

Menke, W., Zha, Y., Webb, S. C., & Blackman, D. K. (2015). Seismic anisotropy indicates ridge-parallel asthenospheric flow beneath the Eastern Lau Spreading Center. *Journal of Geophysical Research: Solid Earth*, *120*, 976–992. https://doi.org/10.1002/2014JB011154

Montagner, J.-P. (2007). Deep Earth structure—Upper mantle structure from isotropic and anisotropic elastic tomography. In: Schubert, G. (Ed.). *Treatise on Geophysics*, *1*, 559–589. https://doi.org/10.1016/B978-044452748-6/00018-3

Okaya, D. A., & McEvilly, T. V. (2003). Elastic wave propagation in anisotropic crustal material possessing arbitrary internal tilt. *Geophysical Journal International*, *153*, 344–358. https://doi.org/10.1046/j.1365-246X.2003.01896.x

Ribe, N. M. (1989). Seismic anisotropy and mantle flow. *Journal of Geophysical Research*, *94*, 4213–4223. https://doi.org/10.1029/JB094iB04p04213

Ribe, N. M. (1992). On the relation between seismic anisotropy and finite strain. *Journal of Geophysical Research*, *97*, 8737–8747. https://doi.org/10.1029/92JB00551

Russo, R. M., & Silver, P. G. (1994). Trench-parallel flow beneath the Nazca plate from seismic anisotropy. *Science*, *263*, 1105–1111. https://doi.org/10.1126/science.263.5150.1105

Smith, G. P., Wiens, D. A., Fischer, K. M., Dorman, L. M., Webb, S. C., & Hildebrand, J. A. (2001). A complex pattern of mantle flow in the Lau backarc. *Science*, *292*, 713–716. https://doi.org/10.1126/science.1058763

Wei, S. S., Wiens, D. A., van Keken, P. E., & Cai, C. (2017). Slab temperature controls on the Tonga double seismic zone and slab mantle dehydration. *Science Advances*, *3*, e1601755. https://doi.org/10.1126/sciadv.1601755

Wei, S. S., Wiens, D. A., Zha, Y., Plank, T., Webb, S. C., Blackman, D. K., Dunn, R. A., et al. (2015). Seismic evidence of effects of water on melt transport in the Lau back-arc mantle. *Nature*, *518*, 395–398. https://doi.org/10.1038/nature14113